Observation of Edge Instability Limiting the Pedestal Growth in Tokamak Plasmas

A. Diallo,[1] J. W. Hughes,[2] M. Greenwald,[2] B. LaBombard,[2] E. Davis,[2] S-G. Baek,[2] C. Theiler,[2] P. Snyder,[3] J. Canik,[4] J. Walk,[2] T. Golfinopoulos,[2] J. Terry,[2] M. Churchill,[2] A. Hubbard,[2] M. Porkolab,[2] L. Delgado-Aparicio,[1] M. L. Reinke,[2] A. White,[2] and Alcator C-Mod team

[1]*Princeton Plasma Physics Laboratory, Princeton, New Jersey 08543, USA*

[2]*Plasma Science and Fusion Center, Massachusetts Institute of Technology, Cambridge, Massachusetts 02139, USA*

[3]*General Atomics, San Diego, California 92186, USA*

[4]*Oak Ridge National Laboratory, Oak Ridge, Tennessee 37831, USA*

(Received 15 October 2013; published 17 March 2014)

With fusion device performance hinging on the edge pedestal pressure, it is imperative to experimentally understand the physical mechanism dictating the pedestal characteristics and to validate and improve pedestal predictive models. This Letter reports direct evidence of density and magnetic fluctuations showing the stiff onset of an edge instability leading to the saturation of the pedestal on the Alcator C-Mod tokamak. Edge stability analyses indicate that the pedestal is unstable to both ballooning mode and kinetic ballooning mode in agreement with observations.

DOI: 10.1103/PhysRevLett.112.115001 PACS numbers: 52.35.-g, 52.25.Xz, 52.30.-q

High performance operational regimes in fusion devices are characterized by the spontaneous formation [1] of steep gradients and stair-step like profiles in density and temperature at the plasma edge (often termed as "*H*-mode pedestal"). These gradients are the result of an edge transport barrier, believed to be caused by the shear-flow suppression of turbulence [2,3], leading to an overall performance enhancement of fusion devices such as tokamaks. As in most physical systems with significant gradients, however, instabilities can arise due to the available source of free energy. In tokamaks, repetitive instabilities termed edge-localized modes (ELM) occur when the pedestal pressure and/or current exceed critical values for a given profile characteristic width scale.

It is well known that the *H*-mode pedestal pressure or current builds between ELMs and collapses during ELMs; this collapse reduces the overall fusion performance. To optimize fusion performance, it is imperative to simultaneously avoid ELMs while maximizing the pedestal. Indeed, the projected fusion performance is correlated with the pressure at the pedestal top [4]. Therefore, an understanding of the pedestal gradients and dynamics is required for validating and improving existing predictive models for projecting future performance on fusion devices such as ITER.

At present, the EPED model (not an acronym) is the leading candidate for predicting the pedestal [5] in multiple fusion devices including Alcator C-Mod [6]. The underlying hypotheses of this model rely on several classes of edge instabilities. The first class encompasses macroinstabilities destabilized by excessive pressure gradients ("ideal ballooning modes"), excessive edge current ("kink or peeling modes"), or a combination ("peeling-ballooning modes"). This class of instabilities constrains the pedestal height. The second class is an ion scale, ballooning-type of microinstability that is kinetically destabilized ("kinetic ballooning mode—KBM") [7] and is hypothesized to restrict the local pressure gradient. This latter class of instability is also operative in magnetospheric physical systems where the onset of KBM is thought to play a vital role in global substorm dynamics of the near-Earth magnetotail ([8–10] and references therein). The combination of these two class of instabilities within EPED lead to a unique prediction of the pedestal pressure in tokamaks; to date, however, there has been no strong evidence of the existence of KBM, much less their role in the pedestal dynamics during ELM cycles in tokamaks.

In this Letter, we show direct evidence of an instability limiting the pedestal between ELMs. Using multiple poloidally and toroidally separated fluctuation diagnostics, we present detailed measurements in both density and magnetic fluctuations and link the onset of the instability associated with a clamping of the pedestal temperature. Theoretical stability calculations show that the edge pedestal is KBM and ballooning unstable during the pedestal evolution. Multiple experiments have successfully demonstrated that the pedestal height increases and, in some cases, tends to saturate before the onset of ELM [6,11–14]. The pedestal gradient has been observed to clamp early during an ELM cycle. Previous attempts have been made to identify an instability in the pedestal region during an ELM-free period on the DIII-D tokamak [15] correlated with the pedestal evolution. However, a direct link between saturation of the pedestal with an onset of microinstabilities responsible for heat and/or particle transport leading to this saturation has never been demonstrated.

Experiments were performed on the Alcator C-Mod tokamak heated with 2 MW of ion cyclotron range of

frequency (ICRF) minority heating [16]. Electron density and temperature were measured using the Thomson scattering system [17]. The charge-exchange(CXRS) system [18] provides the edge ion temperature and radial electric field profiles. To enhance the temporal resolution of the electron temperature evolution, electron cyclotron emission (ECE) measurements [19] are obtained at the pedestal.

To better understand the role of fluctuations in the pedestal dynamics, we investigate both local and global fluctuations during the ELM cycle. The main diagnostics used to probe the inter-ELM fluctuations are the phase contrast imaging (PCI) (sampling the global fluctuations), and the ordinary-mode reflectometer (O-mode), the gas puff imaging (GPI), and the magnetic probes systems (sampling the local, edge fluctuations). We show below that these measurements (from different diagnostics) are consistent with each other and provide the necessary ingredient for comparison with theoretical predictions of the KBM scalings between ELMs.

C-Mod's PCI diagnostic measures the line-integrated absolutely calibrated electron density fluctuations along 32 radially spaced, vertically viewing chords [20]. With these radially spaced chords, a spatial Fourier transform is obtained. Figure 1(a) displays the spectrum $S(k_R, \mathrm{f})$ as a function of frequency and major radius wave number. Beside the broadband fluctuations in this figure, two coherent peaks at 300 kHz and at $k_R = \pm(1.5 \pm 0.5)\,\mathrm{cm}^{-1}$ are observed from which a phase velocity (ω/k) of ± 12 km/s is determined. The phase velocity and the symmetry of the coherent features circled in Fig. 1 suggest a mode localized in the edge having a predominant k_θ, with the opposing signs corresponding to the bottom and top of the PCI beam path.

To improve on the radial localization, we used the O-mode multichannel fixed-frequency reflectometer system to probe the edge electron density fluctuations [21]. Figure 2(a) indicates the fixed frequencies associated with density cutoff layers. Although the absolute density fluctuation levels are difficult to assess, the complex signals from each channel sampling the edge density provide measurements of the fluctuation characteristics at corresponding radii. Figures 2(b)–2(c) display the spectrogram of the complex signals between ELMs. It is observed that the channel probing the density pedestal region (steep gradient region) exhibits coherent fluctuations that onset during the pedestal evolution. The channel probing the pedestal top, on the other hand, does not display any spectral features, indicating that the mode is localized in the steep gradient region.

The 2D measurements of the edge fluctuations are performed using the HeI gas-puff imaging (GPI) system (details of this system can be found in Ref. [22] and references therein). The GPI views the low-field side spanning a 2D cross section area of 3.5 cm (radial) by 3.9 cm (poloidal). The collected HeI emission ($\lambda = 587.6$ nm) is detected by an array of avalanche photodiodes. Figure 3 shows the density fluctuation measurements represented as the conditional spectrum $[S(k_\theta|f)]$ for radii spanning the edge region. These spectra exhibit a coherent fluctuation at 300 kHz peaking at $k_\theta = 0.7\ \mathrm{cm}^{-1}$, propagating in the electron diamagnetic direction in the laboratory frame. Figures 3(a)–3(c) indicate that the mode is undetected in the far scrape-off layer but appears to be dominant near the separatrix.

The characterization of this instability relies on the magnetic component associated with the edge density fluctuations presented above. Such characterization is performed using a double-head magnetic probe held at a fixed position 2 cm away from the separatrix. Note this proximity to the separatrix is a first and was found to be key in the identification of the instability. The two magnetic heads are separated poloidally by 5 mm enabling the resolution of the poloidal wave number spectrum. Figure 4 displays the inter-ELM magnetic $\tilde{B}_\theta$ fluctuations

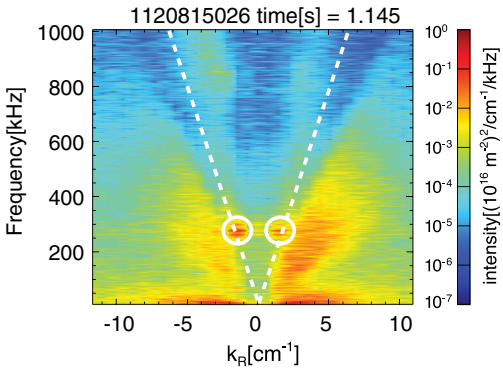

FIG. 1 (color online). (a) Wave number vs frequency spectrum of observed PCI fluctuations displaying a mode coherent in both frequency and radial wave number. From this spectrum, we determine a phase velocity of ± 12 km/s as labeled with the oblique dotted lines.

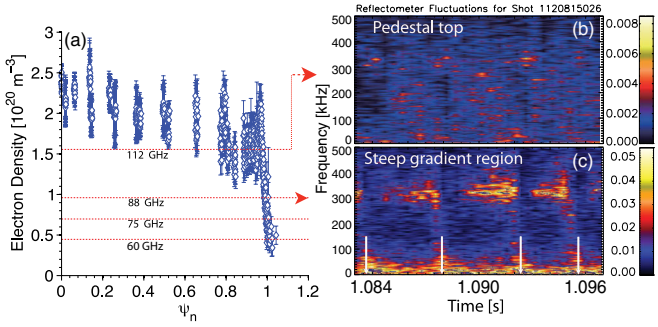

FIG. 2 (color online). Radial localization of the coherent fluctuations. (a) Density profile and overlayed are the vertical lines indicating the density cutoff corresponding to each probing frequency. (b) Spectrogram of the reflectometer signals for the 112 GHz channel probing the pedestal top. (c) This panel shows inter-ELM coherent fluctuations. Note the white vertical lines at the bottom of this panel represent the ELMs.

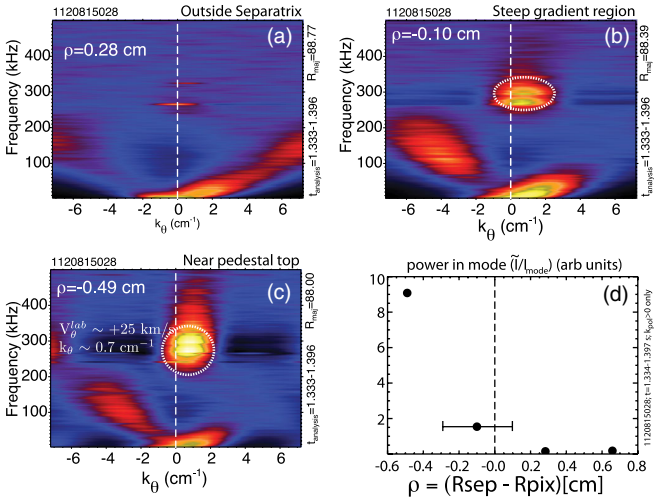

FIG. 3 (color online). Frequency vs wave number spectra of the 2D GPI fluctuations at three different radial locations (a) at $\rho = 0.2$ cm, which is thought to be outside the separatrix; (b) $\rho = -0.10$ cm corresponds to the steep gradient region; and (c) $\rho = -0.49$ cm is located near the pedestal top. Note that with 1–2 cm uncertainties in the pixel registrations and location of the separatrix, the three locations span the edge. (d) Spectral power of the mode as a function of radii.

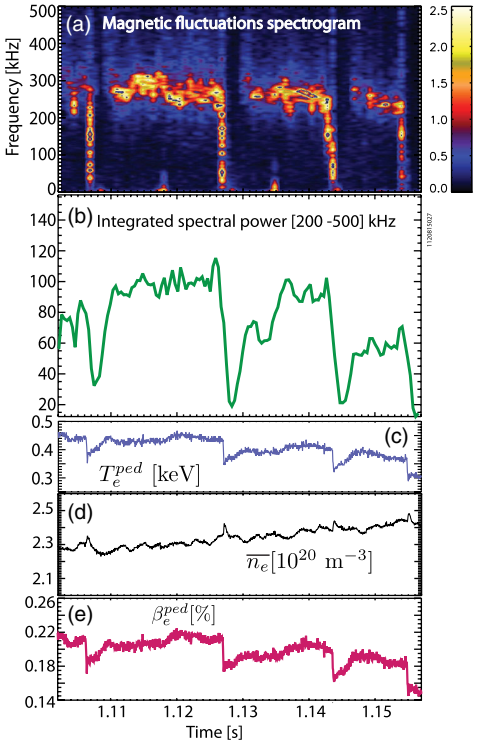

FIG. 4 (color online). (a) Magnetic fluctuations spectrogram displaying the inter-ELM fluctuations sustained for 10–20 ms. (b) Integrated spectral amplitude obtained from integrating the above spectrogram between 200 and 500 kHz. (c) Edge temperature evolution measured using the ECE. (d) Line-averaged density evolution. (e) Estimate of the pedestal electron β evolution.

clearly showing in panel (a) the onset of the coherent fluctuations. This is further highlighted in panel (b) where the integrated power over the frequency band (200 and 500 kHz) shows an increase followed by a saturation of the integrated power. In panel (c), the electron cyclotron emission (ECE) diagnostic shows a prompt drop in the electron temperature (T_e^{ped}) at each ELM, measured at a location just inside the pedestal top. Each ELM event is followed by a period of T_e^{ped} increase, then saturation. The mode turn on is correlated with the pedestal temperature saturation. This saturation persists until the next ELM. This behavior is consistent with a pedestal (of roughly fixed width) having a gradient that is relaxed by ELMs and limited between ELMs by the onset of the observed mode. Combining density [see Fig. 2(d)] and temperature at the pedestal to compute the pressure pedestal (P_e^{ped}), the inter-ELM fluctuations are presented in terms of the electron $\beta = 2\mu_0 P_e^{\mathrm{ped}}/B^2$ at the pedestal in panel (e), confirming the β sensitivity of the onset of instability, consistent with both the KBM and microtearing instabilities.

From the double-head probe, we display in Fig. 5 the poloidal wave number $\tilde{B}_\theta$ fluctuation spectra during the inter-ELM phase. Early in the inter-ELM phase, a broadband wave number structure, as indicated in the left panel of Fig. 5, is observed which later through the ELM cycle becomes coherent in frequency and wave number (see right panel of Fig. 5). The poloidal wave number k_θ ranges between 0.6 and 0.7 cm^{-1}, yielding $k_\theta \rho_s \sim 0.04$ propagating with phase velocity of 30 km/s in the electron diamagnetic direction. Here, $\rho_s = \sqrt{m_i T_e}/(eB)$ defines the Larmor radius with the ion mass m_i, elementary charge e, electron temperature T_e, and magnetic field B.

To reconcile the wave number measurements from the diagnostics covering the poloidal direction, Fig. 6 summarizes the expected k_θ as a function of vertical position. In this figure, the poloidal wave numbers obtained from PCI, GPI, and magnetic probes are plotted as a function of vertical position (equivalent to the poloidal angle). The solid line represents the expected result for a field-aligned perturbation. Figure 6 indicates agreement (within errors) between the various wave number measurements, which

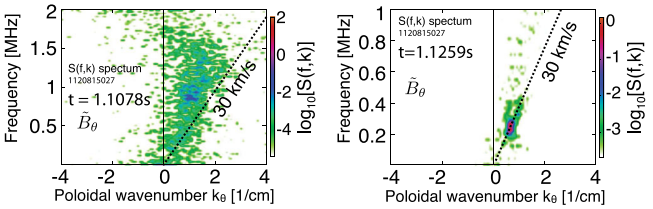

FIG. 5 (color online). Frequency vs wave number spectra of the magnetic fluctuations for two distinct time slices; [Left]: before the onset of instability and [right]: saturated regime. In both panels, an oblique lines is displayed to show the corresponding phase velocity of 30 km/s.

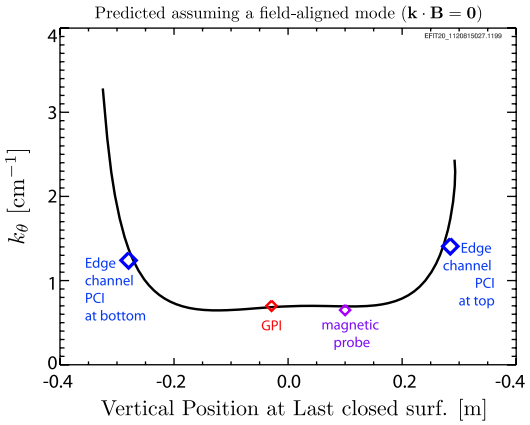

FIG. 6 (color online). Predictions of the poloidal wave number as a function of the vertical position assuming that the instability is field aligned. Overlayed are the vertical positions of the different diagnostics used in this work to show agreement in wave numbers.

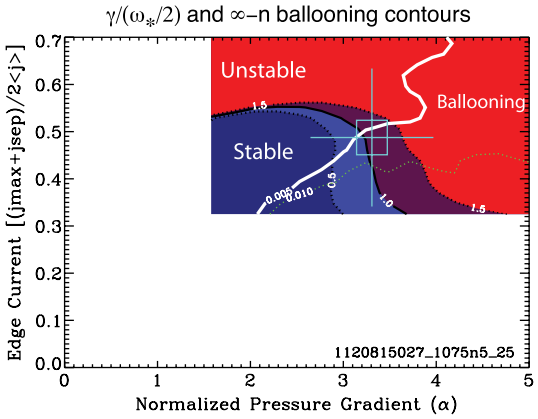

FIG. 7 (color online). Stability contours. The colored contour represents the peeling-ballooning growth rate (γ) normalized to $1/2$ the diamagnetic frequency (ω_*). The discharge operating point is represented by the box with error bars. This point is ballooning unstable. The white line represents the infinite-n ballooning (proxy for the KBM stability) boundary indicating that the operating point is also KBM unstable.

yields a $n = 10$ field-aligned mode consistent with ballooning characteristics.

The theory of stability of the edge pedestal, embodied in the ELITE code [23], allows us to determine the stability characteristics before the onset of ELMs. In addition, using the infinite-n ballooning stability criteria, a proxy for KBM stability, we can determine the pedestal stability to KBMs. We have performed peeling-ballooning stability calculations for the ELMy discharge using the same technique employed previously in [24]. Note that these stability calculations depend on the full radial structure of the current and pressure profiles. The results are shown Fig. 7. Within the error bars, the operating point for the discharge is on the ballooning boundary; this is characteristic of C-Mod ELMy discharges. In addition, the stability boundaries for the KBM proxy are shown, indicating that the operating point is infinite-n unstable which is equivalent to being KBM unstable. The edge stability analysis predicts that pedestal is both KBM and ballooning unstable consistent with the experimental observations.

In summary, this Letter reports edge fluctuation measurements during the pedestal evolution, and comparison with model predictions. We observed, using multiple poloidally separated edge diagnostics, coherent edge density fluctuations with associated magnetic signature. Furthermore, the coherent fluctuations onset during an increase of the pedestal temperature, which in turn, saturates until the next ELM. This observation is consistent with the fluctuations enhancing the edge transport limiting the growth of the pedestal temperature. Characterization of these coherent fluctuations in frequency and wave number shows that the mode propagates in the electron diamagnetic direction in the laboratory frame with ion spatial $k_\theta\rho_s \sim 0.04$. In addition, the mode is radially localized at the edge pedestal and is field aligned (as it is observed by multiple diagnostics, all of which provide wave numbers consistent with $\mathbf{k}\cdot\mathbf{B} = 0$). Finally, the mode's stiff onset is shown to be sensitive to the electron β_e which is a key magnetic signature of the KBM or microtearing mode. An important additional characteristic distinguishing the two instabilities is the propagation direction. Assuming that the observed mode is located in the minimum of the radial electric field well and accounting for instrumental effects of the CXRS diagnostic and the "barberpole" effect [25], we determine the plasma frame phase velocity of the mode to be (7 ± 6) km/s, which is in the ion diamagnetic drift direction. Thus, this would be compatible with KBM and inconsistent with an electron mode such as microtearing. This compatibility was corroborated using linear gyrokinetic calculations GS2 (not shown here) over a limited radial range within the pedestal, where KBM is dominant at a similar $k_\theta\rho_s = 0.03$ to that of the mode measured.

For its predictive capability of future machine pedestal height and width, EPED hypothesized that the pedestal gradient is limited by the onset of the KBM. We have shown for the first time the onset of a coherent fluctuation (exhibiting the same characteristics as KBM) associated with an increase of the pedestal temperature. Once the mode is turned on, the pedestal temperature remains clamped until the next ELM. Further investigations should focus on comparisons with gyrokinetic and gyrofluid simulations estimates of the transport provided by this coherent mode.

The authors thank A. Bhattacharjee, R. Maingi, and W. Guttenfelder for useful discussions and the Alcator C-Mod operation group for expert running of the tokamak. This work was supported at PPPL by DoE Grant No. DE-AC02-09CH11466, at MIT by DoE Contract No. DE-FC02-99ER54512, and in part by an appointment to the U.S. DOE Fusion Energy Postdoctoral Research Program administered by ORISE.

[1] F. Wagner, G. Fussmann, T. Grave, M. Keilhacker, M. Kornherr, K. Lackner, K. McCormick, E. R. Müller, A. Stäbler, G. Becker, *et al.*, Phys. Rev. Lett. **53**, 1453 (1984).
[2] P. Terry, Rev. Mod. Phys. **72**, 109 (2000).
[3] K. H. Burrell, Phys. Plasmas **4**, 1499 (1997).
[4] J. Kinsey, G. Staebler, J. Candy, R. Waltz, and R. Budny, Nucl. Fusion **51**, 083001 (2011).
[5] P. Snyder, R. Groebner, J. Hughes, T. Osborne, M. Beurskens, A. Leonard, H. Wilson, and X. Xu, Nucl. Fusion **51**, 103016 (2011).
[6] J. Walk, P. Snyder, J. Hughes, J. Terry, A. Hubbard, and P. Phillips, Nucl. Fusion **52**, 063011 (2012).
[7] J. W. Connor, R. J. Hastie, and J. B. Taylor, Phys. Rev. Lett. **40**, 396 (1978).
[8] C. Z. Cheng and A. T. Y. Lui, Geophys. Res. Lett. **25**, 4091 (1998).
[9] P. Zhu, C. R. Sovinec, C. C. Hegna, A. Bhattacharjee, and K. Germaschewski, J. Geophys. Res. **112**, A06222 (2007).
[10] A. Bhattacharjee, Z. W. Ma, and X. Wang, Geophys. Res. Lett. **25**, 861 (1998).
[11] A. Kirk, H. R. Wilson, G. F. Counsell, R. Akers, E. Arends, S. C. Cowley, J. Dowling, B. Lloyd, M. Price, M. Walsh, *et al.*, Phys. Rev. Lett. **92**, 245002 (2004).
[12] H. Urano, T. Takizuka, Y. Kamada, N. Oyama, and H. Takenaga, and the JT-60 Team, Nucl. Fusion **48**, 045008 (2008).
[13] R. J. Groebner, T. H. Osborne, A. W. Leonard, and M. E. Fenstermacher, Nucl. Fusion **49**, 045013 (2009).
[14] A. Diallo, R. Maingi, S. Kubota, A. Sontag, T. Osborne, M. Podestà, R. Bell, B. LeBlanc, J. Menard, and S. Sabbagh, Nucl. Fusion **51**, 103031 (2011).
[15] Z. Yan, G. R. McKee, R. J. Groebner, P. B. Snyder, T. H. Osborne, M. N. Beurskens, and K. H. Burrell, Phys. Plasmas **18**, 056117 (2011).
[16] S. J. Wukitch, Y. Lin, A. Parisot, J. C. Wright, P. T. Bonoli, M. Porkolab, N. Basse, E. Edlund, A. Hubbard, L. Lin, *et al.*, Phys. Plasmas **12**, 056104 (2005).
[17] J. W. Hughes, D. Mossessian, K. Zhurovich, M. DeMaria, K. Jensen, and A. Hubbard, Rev. Sci. Instrum. **74**, 1667 (2003).
[18] R. M. Churchill, C. Theiler, B. Lipschultz, R. Dux, T. Putterich, and E. Viezzer A. C.-M. Team, and A. U. Team, Rev. Sci. Instrum. **84**, 093505 (2013).
[19] P. J. OShea, A. E. Hubbard, Alcator C-Mod Group, in *Proceedings of 9th Joint Workshop on ECE and ECRH, Borrego Springs, 1995*, edited by J. Lohr (World Scientific Publishing Co, Singapore, 1995), p. 7.
[20] L. Lin, M. Porkolab, E. Edlund, J. Rost, M. Greenwald, N. Tsujii, J. Candy, R. Waltz, and D. Mikkelsen, Plasma Phys. Controlled Fusion **51**, 065006 (2009).
[21] A. Dominguez, Ph. D. thesis, Massachusetts Institute of Technology, 2012.
[22] I. Cziegler, J. L. Terry, J. W. Hughes, and B. LaBombard, Phys. Plasmas **17**, 056120 (2010).
[23] P. B. Snyder, H. R. Wilson, J. R. Ferron, L. L. Lao, A. W. Leonard, T. H. Osborne, A. D. Turnbull, D. Mossessian, M. Murakami, and X. Q. Xu, Phys. Plasmas **9**, 2037 (2002).
[24] T. H. Osborne, P. B. Snyder, K. H. Burrell, T. E. Evans, M. E. Fenstermacher, A. W. Leonard, R. A. Moyer, M. J. Schaffer, and W. P. West, J. Phys. Conf. Ser. **123**, 012014 (2008).
[25] Note: This effect manifests itself when measuring the poloidal velocity in the laboratory frame and the plasma is toroidally rotating. One needs to unfold this effect in our case. This apparent poloidal velocity in the laboratory frame is $V^*_{\mathrm{pol}} = V_{\mathrm{pol}} - V_{\mathrm{tor}} \tan(\alpha) + V_{\mathrm{phase}}$, where α is the pitch angle, V_{tor} is toroidal velocity, and V_{phase} is the phase velocity of a mode.